Universality of amplitude combinations in two-dimensional percolation

2000 J. Phys. A: Math. Gen. 33 1113

(http://iopscience.iop.org/0305-4470/33/6/303)

J. Phys. A: Math. Gen. **33** (2000) 1113–1137. Printed in the UK PII: S0305-4470(00)06524-0

Universality of amplitude combinations in two-dimensional percolation

Daniel Daboul†, Amnon Aharony† and Dietrich Stauffer‡

† School of Physics and Astronomy, Beverly and Raymond Sackler Faculty of Exact Sciences, Tel Aviv University, 69978 Tel Aviv, Israel
‡ Institute of Theoretical Physics, Cologne University, 50923 Köln, Germany

E-mail: daboul@fractal.tau.ac.il

Received 2 August 1999

Abstract. We generated/extended low concentration series for the second moment of distances between cluster points A_2 in site and bond percolation on the square lattice and used them to calculate series for the correlation length ξ. We analysed these and other series for their critical amplitudes, and compared them with results from Monte Carlo simulations of triangular site, square site, and square bond percolation. The values obtained from the different models for the amplitude combination $B^2\xi_0^2/\Gamma_2$ (ξ_0, Γ_2, and B are the amplitudes of ξ, the second moment of the cluster size distribution M_2, and the strength of the infinite cluster P, respectively), are all within the range 2.23 ± 0.10, confirming universality.

1. Introduction

Percolation models have been studied for decades and have been used to describe geometric phase transitions in a large variety of systems [1–3]. Scaling theory, originally developed for thermodynamic phase transitions, has been successfully formulated for percolation. It predicts the universality of the critical exponents and certain scaling relations among them. For the critical amplitudes, which are not universal by themselves, it further predicts the universality of certain ratios and other multiplicative combinations [4].

In particular in two dimensions much knowledge has accumulated: the critical exponents are known exactly, and the non-universal critical threshold p_c is known exactly for some lattices and very accurately for many others. Amplitudes were also estimated for some quantities in some models, but here the data are not complete.

In this paper we present new estimates for the critical amplitude ξ_0 of the connectivity length ξ for bond percolation (with site and bond counting), with the aim to calculate the combination $\xi_0^d B^2/\Gamma_2$, which is predicted to be universal. Here, B and Γ_2 are the amplitudes of the strength of the infinite cluster P and the second moment of the cluster size distribution M_2, respectively, and d is the dimension restricted to 2 throughout this paper. We further obtain all these amplitudes for bond and site percolation, using series expansions and Monte Carlo simulations, and compare our values with those from previous publications. This comparison turns out to be non-trivial and shows that one cannot simply combine the numerical values from different papers, since different researchers use slightly different definitions and normalizations.

0305-4470/00/061113+25$30.00

Section 2 gives the precise definitions of the quantities we calculate and explains how their power series were generated. In section 3 we carefully introduce the three models under study and address the problem of choosing the proper unit lengths and normalizations for cluster counting. Section 4 is devoted to the series analysis, while section 5 gives details about our Monte Carlo simulations. The value of universal quantities can be useful to calculate additional *non-universal* quantities in models, where only some of them are known. We further discuss this and summarize our results in section 6.

2. Generation of the series

The generation of the low concentration series for the moments of the cluster size distribution M_k is based on the equation

$$M_k(p) = \sum_{b=0}^{\infty} \sum_{\Gamma \in \Gamma_b} p^b (1-p)^{t(\Gamma)} s(\Gamma)^k \tag{1}$$

which is given here for the case of bond percolation with site counting. Here Γ_b denotes the set of all clusters with b bonds, $s(\Gamma)$ the number of sites in cluster Γ, $t(\Gamma)$ its number of perimeter bonds, and p is the bond concentration, meaning the probability that a certain bond is occupied. In practice one cannot perform the summation for b up to infinity, but has to restrict oneself to $b \leqslant N$ with a finite N. Often it is convenient to use the variable $q = 1 - p$, which becomes the expansion parameter in high concentration series. The generalization to site percolation, or bond percolation with bond counting, is obvious.

An expansion of the quantities to order N is calculated by summing up the contributions from all clusters with up to N bonds. The corresponding equation for the kth moment of distances is

$$A_k(p) = \sum_{b=0}^{\infty} \sum_{\Gamma \in \Gamma_b} p^b (1-p)^{t(\Gamma)} \sum_{i,j=1}^{s(\Gamma)} r_{ij}^k \tag{2}$$

where s^k is replaced by $\sum_{i,j=1}^{s(\Gamma)} r_{ij}^k$, and r_{ij} denotes the geometrical distance between sites i and j of the cluster Γ†.

A computer program was used to enumerate all different cluster configurations recursively, by an algorithm similar to those described in [5–7], for clusters with up to N bonds. Their contribution to all the relevant orders of the series was then calculated, and added to the coefficients.

In the site case this was the only method used, and the correctness of the program was checked by re-generating the series of the moments given in [8] and also the series for the calliper diameter of branched polymers [9], which is a more rigorous check, since it includes the geometrical shape of every cluster.

In the bond-percolation cases, a different program calculated the same series from shape data files (of up to 14 bonds) [10], where each entry contains the complete geometrical information about a cluster shape together with the number of distinct configurations (reflections, rotations) in which it appears. This approach reduces the amount of computer time needed if many series are generated, but is not really a different technique since the shape lists were obtained using the same algorithm as mentioned above. Correctness of the algorithms was checked completely to order 11 by comparison with series and data files by Wan *et al* [11], and to a lesser extent to all orders used, by the regeneration of series in [12]. Based on these

† Note that in equation (47*b*) of Stauffer and Aharony [1] the R_s^2 was meant to be averaged over all cluster configurations with the proper weights as done here in (2); this was clarified by R M Ziff (1998 private communication).

Table 1. Series for bond percolation with bond counting. ($P(q)$ and $M_2(p)$ after [8].)

n	Coefficients a_n in $\ldots = \sum_n a_n q^n$ or $\ldots = \sum_n a_n p^n$, respectively $P(q)$	$M_2(p)$	$A_2(p)$	$\xi^2(p)$
0	1	0	0	0
1	−1	1	0	8
2	0	6	16	32
3	0	18	160	96
4	0	48	864	320
5	0	126	3 712	632
6	−1	300	13 648	2 704
7	1	762	46 592	2 136
8	−8	1 668	145 776	23 296
9	14	4 216	443 936	−11 384
10	−54	8 668	1 265 040	203 712
11	114	21 988	3 591 584	−278 044
12	−345	43 058	9 622 440	1 655 152
13	787	110 832	26 054 640	−2 872 568
14	−2 203	202 432	66 675 360	11 503 792
15	5 483	561 020	174 991 936	
16	−15 283	875 382		
17	39 891	2881 286		
18	−108 216	3501 056		
19	280 506			
20	−739 374			
21	1 919 390			
22	−5 084 644			
23	13 447 658			
24	−35 886 008			
25	95 206 424			
26	−253 035 652			
27	671 219 234			
28	−1 786 728 606			
29	4 756 022 606			
30	−12 671 128 640			
31	33 729 167 216			
32	−89 882 252 217			
33	239 775 402 139			
34	−640 561 757 069			
35	1 711 651 978 489			
36	−4 574 053 238 290			
37	12 223 988 780 968			
38	−32 689 762 102 187			
39	87 483 151 484 487			

checks, we strongly believe that the new series presented in this paper (tables 1–3), namely the second moment of distances A_2 and the squared correlation length $\xi^2 = A_2/M_2$, are correct.

Other series we use in this paper are the long high concentration M_1 and the low concentration M_2 series for site percolation and for bond percolation with bond counting, published by Conway and Guttmann [8]. The moments M_k for the bond-percolation model with site counting were previously studied with series in general dimension by Adler *et al* [12]. However, these papers do not deal with quantities that, like A_k and ξ, depend on the *geometrical shape of the clusters*.

Table 2. Low concentration series for bond percolation with site counting. ($M_2(p)$ after [12].)

	Coefficients a_n in $\ldots = \sum_n a_n p^n$		
n	$M_2(p)$	$A_2(p)$	$\xi^2(p)$
0	1	0	0
1	4	4	4
2	12	32	16
3	36	164	52
4	88	688	144
5	236	2 540	412
6	528	8 540	940
7	1 392	27 192	2 840
8	2 828	81 308	4 876
9	7 608	237 656	18 952
10	14 312	658 916	18 308
11	39 348	1 821 844	129 876
12	6 970	4 788 356	8 500
13	197 620	12 739 444	948 036
14	318 232	32 109 712	−877 136
15	1013 424	83 317 120	7794 256

We study the quantities near the critical threshold, where we are interested in the critical amplitudes as defined by the following asymptotic expressions:

$$M_2(p) \sim \Gamma_2(p_c - p)^{-\gamma} \tag{3}$$

$$P(q) = p - M_1(p) \sim B(p - p_c)^{\beta} \tag{4}$$

$$\xi \sim \xi_0(p_c - p)^{-\nu}. \tag{5}$$

With these definitions, the combination $\xi_0^d B^2/\Gamma_2$ is expected to be universal [4]. Note that in the literature there exists a large variety of different definitions and normalizations of quantities relevant to percolation, in particular their amplitudes. For instance in [8] the authors use $P = 1 - M_1/p$, and in the bond-counting case all their series include a factor of 2 compared with ours. Such details obviously influence the numerical value obtained for an amplitude, and one must stick to consistent definitions, and calculate conversions properly.

3. Details of the differences between the models

Figure 1 will help us to explain the differences between the models we address. It has three parts labelled A, B and C, each of which shows a section of the square lattice. These parts represent the bond-percolation model with site counting, the bond-percolation model with bond counting, and the site-percolation model, respectively [13]. In each of the parts we have a finite cluster (lattice animal), and at first sight these clusters look quite similar (T-shaped). For each model however the 'cluster' is different, as we demonstrate by calculating its contribution to M_2.

Bond-percolation model with site counting or bond counting. Here all lattice sites are occupied, and bonds, which are occupied with probability p, form the clusters.

The configuration shown has three bonds, four sites, and a bond perimeter of 10, hence when counting sites its contribution to M_2 is $p^3(1-p)^{10}4^2$. If we interpret this figure as representing the shape rather than the configuration, it appears in four orientations, and thus this contribution appears four times. More accurately phrased we count the configurations per

Table 3. Series for site percolation with site counting. ($P(q)$ and $M_2(p)$ after [8].)

	Coefficients a_n in $\ldots = \sum_n a_n q^n$ or $\ldots = \sum_n a_n p^n$, respectively			
n	$P(q)$	$M_2(p)$	$A_2(p)$	$\xi^2(p)$
0	1	0	0	0
1	−1	1	0	4
2	0	4	4	16
3	0	12	32	36
4	−1	24	148	96
5	1	52	528	244
6	−4	108	1 652	432
7	−4	224	4 688	908
8	−15	412	12 364	2 392
9	−5	844	311 76	3 344
10	−158	1 528	75 264	8 168
11	234	3 152	176 808	14 084
12	−1 349	5 036	399 812	41 472
13	2 713	11 984	902 432	−540
14	−13 704	15 040	1 938 596	269 784
15	42 676	46 512	4 272 328	−213 012
16	−172 825	34 788	8 741 148	1414 560
17	559 053	197 612	19 243 904	−2449 812
18	−2 029 776	4 036	37 002 332	
19	6 774 936	929 368		
20	−23 900 386	−702 592		
21	81 129 962	4 847 552		
22	−282 099 620	−7 033 956		
23	963 894 132	27 903 296		
24	−3 331 512 669	−54 403 996		
25	11 422 580 633	170 579 740		
26	−39 350 336 472			
27	134 939 821 080			
28	−463 383 554 563			
29	1586 767 676 943			
30	−5434 335 886 108			

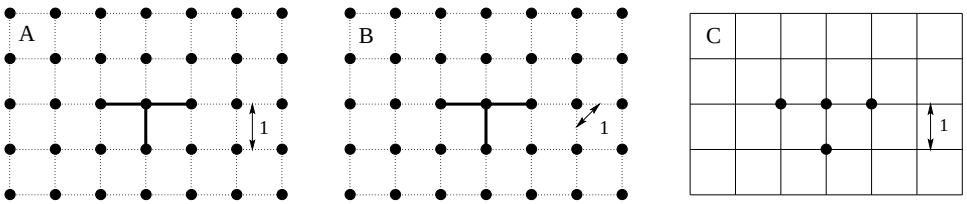

Figure 1. Illustration of the different percolation models under study: (A) bond percolation with site counting, (B) bond percolation with bond counting, (C) site percolation (site counting). The double-sided arrow indicates the unit length.

total number of *sites* on the lattice (rather than per number of bonds) since we deal with site counting. Due to the fact that all sites are occupied we need to take single sites into account as zero-bond clusters, contributing $(1-p)^4$.

In the case of *bond counting* the shown configuration contributes $p^3(1-p)^{10}3^2$. Now we have to normalize by the total number of *bonds* on the lattice, hence this shape contributes twice. The contribution of the single-site cluster evaluates to 0.

Site-percolation model. Here lattice sites are occupied with probability p, and all the bonds are occupied. The configuration shown contributes $p^4(1-p)^8 4^2$, because its site perimeter is 8. Again the shape contributes four times.

For calculating the correlation length one needs to choose the unit length properly in order to recover universality. Our general rule is to choose the unit length such that there is one entity of the counted cluster size (site or bond) per unit area. In figure 1 these lengths are indicated by a double pointer annotated with '1'. Whenever we calculate the distance between sites, this rule naturally reproduces the lattice constant as the proper choice. In the bond percolation problem with bond counting on the square lattice, the distance between the centres of the nearest neighbour bonds has to be set to unity. Less obvious unit lengths apply to other lattices, such as the triangular lattice.

Please note also, that with this choice of unit length our way to count cluster configurations per total number of sites or bonds on the lattice, becomes in each of the cases identical to normalization by lattice area. This is equivalent to the non-trivial statement: 'a cluster of size 1 occupies an area 1 and contributes once!'

4. Analysis of the series

For each of the three models we analysed the three series of $P(q)$, $M_2(p)$ and $\xi^2(p)$. The critical exponents in two-dimensional percolation are known exactly ($\beta = \frac{5}{36} \approx 0.138\,88$, $\gamma = \frac{43}{18} \approx 2.3888$, $\nu = \frac{4}{3} \approx 1.3333$, see e.g. [1]), as well as the threshold in the bond case ($p_c = \frac{1}{2}$). Although the critical threshold is not known exactly for site percolation, the estimate by Ziff [14] of $p_c \approx 0.592\,7460 \pm 0.000\,0005$ is so accurate compared with what could be obtained from the series, that for our purposes it can be treated like an exactly known value.

Nevertheless, before actually addressing the problem of obtaining the critical amplitudes, we analysed each of the series for its critical exponent and threshold. The results gave us a feeling of how well the series behave, and if indeed they point to the correct values. Thus they let us estimate to what degree we can trust the new values for the unknown amplitudes. Since in series expansion one can never completely exclude the possibility of systematic errors, we find that this is a valuable precaution. In general we found the known values to agree with those shown by the series within error estimates from scattered 'data points' alone. More details are given in the following section, where applicable.

For the analysis we used several established techniques, all based on the Padé approximation. Analysis for the critical exponents was done with Dlog Padé analysis (when calculating a Padé approximant to the logarithmic derivative of a series, its first-order real and positive pole closest to the origin in the complex plane gives an estimate for the critical threshold and the corresponding residue gives an estimate for the critical exponent, see e.g. [15]) and in some cases using the techniques known as M1 and M2, which take into account possible non-analytic corrections (see [16, 17] or [12, 18] and references therein).

To get estimates for the critical amplitudes we use our knowledge of the exponents and thresholds, to transform the original series into series for quantities known to have a simple pole at the critical point, with a residue, that allows us to calculate the value of the amplitude. These transformed series are then approximated by Padé functions and we proceed as usual. If, e.g., we have a series for $M_2(p)$, which is expected to diverge as $\Gamma_2(p_c - p)^{-\gamma}$, we could calculate a series for $M_2(p)^{1/\gamma}$, which should behave like $\Gamma_2^{1/\gamma}/(p_c - p)$. Alternatively we could generate a series for $M_2(p)(p_c - p)^{\gamma-1}$ and analyse for a singularity of the type $\Gamma_2/(p_c - p)$. We actually used both approaches, the latter in particular for $P(q)$, and include further details in the following.

Another alternative is to completely divide out the leading singular behaviour (e.g. study $P(q)(q_c - q)^{-\beta}$ or $M_2(p)^{1/\gamma}(p_c - p)$) and evaluate Padé approximants to the resulting series at the true threshold. Such biased estimates usually give the most accurate values if judged from the statistical fluctuations alone. On the other hand, corrections to the leading singular behaviour now gain importance and will lead to systematic deviations from the correct amplitudes, which may well be larger than the fluctuations. A systematic way to account for corrections of the expected form, is to calculate inhomogeneous (biased) differential approximants to the transformed series. In the present paper we do not follow this computationally more complex approach. Instead we show the biased estimates for comparison but base our conclusions on the unbiased estimates.

Analysis shows that all the original series point to an additional non-physical singularity on the negative real axis, at around $p_n \approx -0.3$ to -0.4. In some cases this singularity attracts more Padé approximants' poles than the physical singularity. In any case, convergence of approximants near the latter can be improved by applying an analytic transformation (Euler transformation) to the series, before calculating the Padé approximants. Details of this technique are described in [19]. Such a transformation, of the form $z = p_n\ p/(p_n - p)$, aims to map the non-physical singularity in p far away from the origin, and to reduce its detrimental effect. In cases where we use such a transformation, we try varying its parameter p_n in reasonable ranges to make sure that the results we obtain are not sensitive to the precise form.

4.1. Bond percolation with bond counting

In the case of bond percolation with bond counting we have series for $P(q)$ up to order q^{39} (40 terms), for $M_2(p)$ up to p^{18} (18 terms without the leading zero) (both converted from [8] to suit our definitions) and for $\xi^2(p)$ up to p^{14} (14 terms without the leading zero) as shown in table 1.

In the following we describe in detail the different stages of analysis. As we proceed towards the other models we will skip the details.

Series for $P(q)$. We start with a Dlog Padé analysis of this 40-term series. As a first step we calculate all poles (real and complex, and any order) of all the Padé approximants to the logarithmic derivative of the series ($\mathrm{d}\ln P(q)/\mathrm{d}q$), that are determined fully by the series. They are plotted in the complex plane and the concentration of the real ones is analysed (figure 2(*a*)). The 'strongest' pole (the point attracting the highest number of Padé poles) is indeed 0.5, but a comparable one is observed at around -0.35. Application of an Euler transformation with $p_n = -0.4$, evaluating Padé approximants to the transformed series and re-transforming with the inverse Euler transformation leaves 0.5 as the only noticeable real pole in the range $[-1, 1]$. This is documented by figure 2(*b*).

As the next step one can look at the plot of residues versus first-order real poles obtained from Padé approximants to the $\mathrm{d}\ln P(q)/\mathrm{d}q$-series. The data points in such plots usually do not concentrate only around the true critical values, but instead are spread out along a line that passes through the point defined by the true critical values (figure 3). Here it is understood that, even when applying Euler transformations, we transform the estimates back using the inverse transformation before preparing the plot. This is a convenient form of visualization which avoids confusion. In the case of $\mathrm{d}\ln P(q)/\mathrm{d}q$ the line is well converged and passes through the correct point almost within the scattering range of the points. If we do a biased reading of the q_c-estimates at the known exponent, the value deviates from the true one by at most $q_c/1000$ (see the inset in figure 3). We take this as a rough estimate of how trustworthy

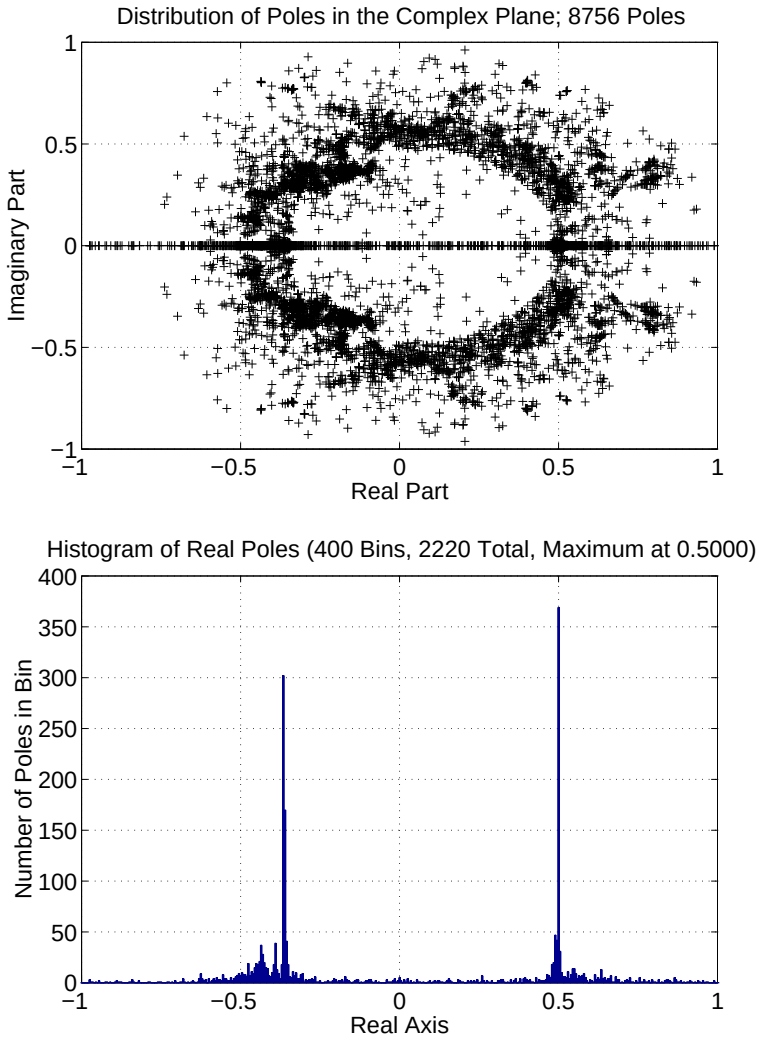

(*a*)

Figure 2. Effect of an Euler transformation on the distribution of poles from all Padé approximants in the complex plane, obtained from the series for $P(q)$ in the bondpercolation (bond-counting) model. (*a*) The distribution for the logarithmic derivative of the series and (*b*) the distribution that results if an Euler transformation with $p_n = -0.4$ is applied to that derivative. The poles are transformed back to the q-plane before plotting.

the value obtained by the amplitude series is, if indeed its convergence is comparable.

To obtain the critical amplitude B, we use our knowledge of the exact β and $q_c = 1 - p_c$ to calculate a series for $P(q)(q_c - q)^{-(1+\beta)}$, which is supposed to behave as $B/(q_c - q)$ near q_c (B-amplitude series in the following). This series can again be conveniently approximated with Padé functions, and the residue of simple real poles directly gives estimates for the critical amplitude B.

The B-amplitude series also shows a negative pole around -0.38, but still convergence in the pole–residue plot is very good (over 500 approximants in a range smaller than $q_c \pm 0.005$).

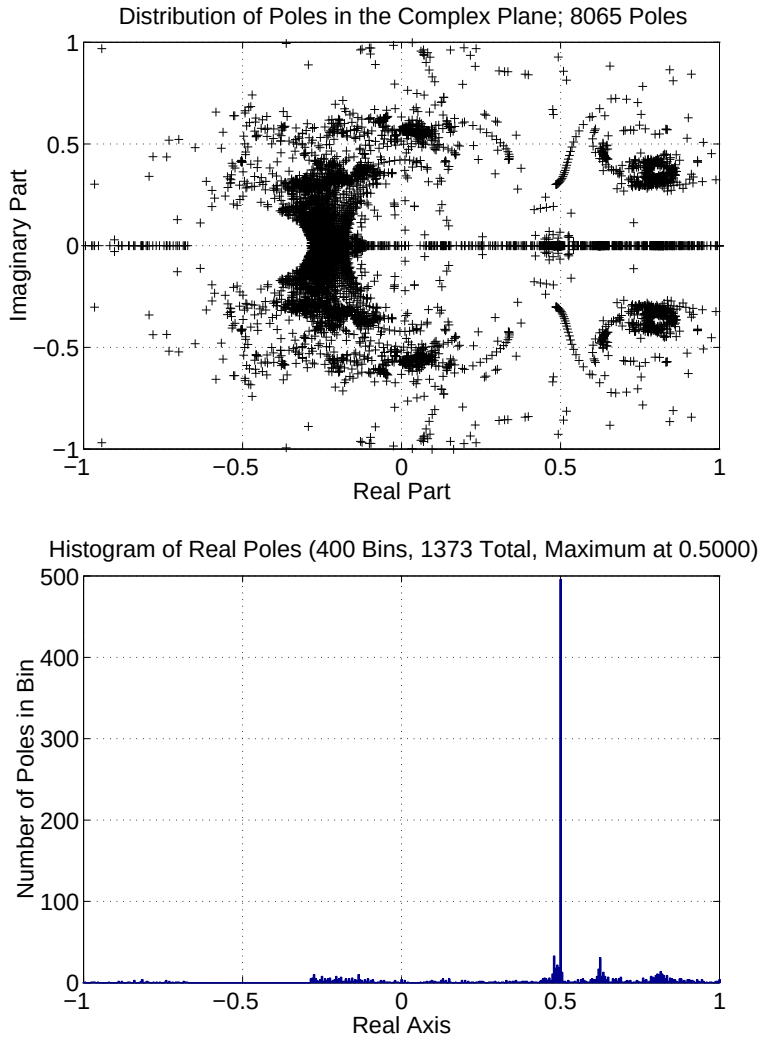

(*b*)

Figure 2. (Continued)

An Euler transformation with $p_n = -0.4$ further improves convergence. Better than usual, the highest concentration of pole–residue points is actually around the exactly known q_c (figure 4). The plot suggests $B = 0.7771 \pm 0.0021$, where the error margin is calculated from the spreading of data points in the range where the density is high (indicated by the box in figure 4). This includes the uncertainty in the q_c value suggested by the $P(q)$ series.

Another form of visualization is to plot the estimates for p_c, the exponent, or the amplitude versus the order of the corresponding Padé approximant (here we call $L + M$ the order of the approximant $[L/M]$). Since longer series correspond to higher orders $L + M$, one expects the points in such plots to eventually converge to the correct value. In our actual plots (e.g. figures 5(*a*) and (*b*)) we use the slightly modified x-coordinates $L + M + (L + M - |L - M|)/(L + M + 1)$. They distribute all approximants of a given

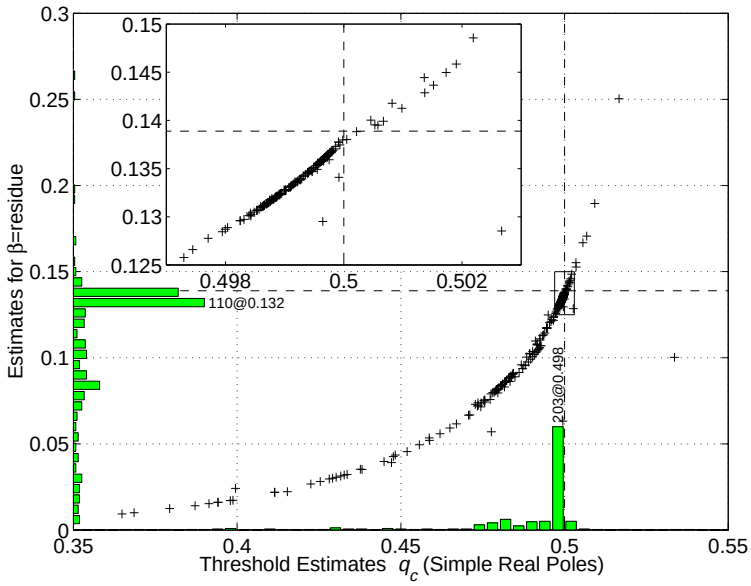

Figure 3. Pole–residue plot from a Dlog Padé analysis of the series of $P(q)$ in the bond-percolation (bond-counting) model. We used an Euler transformation with $p_n = -0.4$. The main part gives an overview over a large region including almost all data points. The histograms on the axes show how these points are distributed. The dashed lines indicate the known values for q_c and β. The inset is an enlarged view of the small region with the highest concentration of points as indicated by the box. For comparison we calculated the average and standard deviation σ_n from the points in the boxed area. This gives the estimates $q_c = 0.499\,35 \pm 0.000\,72$ and $\beta = 0.1344 \pm 0.0032$ with $n = 213$.

order $L + M$ throughout the interval $L + M \leqslant x < L + M + 1$, which causes less data points to be plotted on top of each other and thus enhances the visualization. Another minor effect is that approximants closer to the central ones $[L/L]$, which often give more reliable estimates, are shifted to the right.

In many cases we observe that indeed with increasing order the points converge to a certain value. We then choose limits in the y-direction big enough to enclose the area where many points above some order concentrate, and from all points within this box calculate the average $\langle y \rangle$ and the standard deviation σ_N. These numerical values are summarized in tables 4–6 and are used to determine our final estimates. As we know from other models, e.g. directed percolation [20], where much longer series have been calculated, even when the points seem to have already settled down to a certain value, shifts at higher orders are still possible. However such an analysis is the best we can do with the available data. It appears more systematic to use the error estimates from such plots than from pole–residue plots, because the latter *per se* treat all orders equally.

For q_c and B the plots are shown in figures 5(a) and (b), respectively. Here we did not use any Euler transformation, because it removed especially the poles from the highest-order approximants. Including those estimates from order 28 and above that are not obviously scattered far away from the point of convergence (as indicated by the boxes), we calculate averages of $q_c = 0.499\,994 \pm 0.000\,015$ and $B = 0.777\,71 \pm 0.000\,95$ (see also table 4). The fact that the known value of $q_c = \frac{1}{2}$ lies within the error margins, gives some confidence in the estimates for B obtained from the same series.

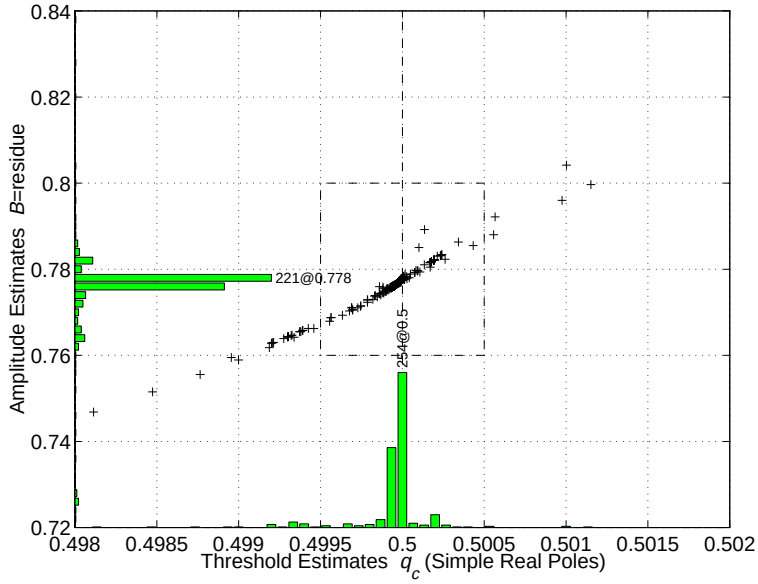

Figure 4. Pole–residue plot from a Padé analysis of the B-amplitude series in the bond-percolation (bond-counting) model. We used an Euler transformation with $p_n = -0.4$. Averaging over the 453 points in the boxed area leads to estimates of $q_c = 0.499\,978 \pm 0.000\,087$ and $B = 0.7771 \pm 0.0021$, where the value behind the '$\pm$' is one standard deviation σ_n. See the caption of figure 3 for further explanation.

Figure 6 shows the analogous plot from biased evaluation of Padé approximants to $P(q)(q_c - q)^{-\beta}$. The box parameters can be read from the figure. The average suggests $B = 0.778\,00 \pm 0.000\,60$.

Series for $M_2(p)$. Again we start with a Dlog Padé analysis of the original 18-term series (divided by p, to get a non-zero constant coefficient), and as before convergence of data points improves by applying an Euler transformation with p_n near -0.3. We already mentioned when discussing the $P(q)$ series, that the line of pole–residue data points does not pass through the point of exactly known threshold and exponent. In the case of the $M_2(p)$-series this also happens, and the offset, although still small, is considerably bigger than for the other series. As can be seen in figure 7(*a*), which shows only a tiny portion of the pole–residue plot, this offset amounts to an error of approximately $p_c/500$.

To see if non-analytic corrections to the leading critical behaviour can explain this deviation, we study the series using the methods M1 and M2, mentioned at the beginning of this section. M2 does not provide any insight; it is not sensitive enough for this series in the region of interest. M1 converges properly, but it does not resolve the offset from $p_c = \frac{1}{2}$ either. Instead, it suggests the values of $p_c = 0.4990 \pm 0.0005$, $\gamma = 2.30 \pm 0.02$, with a value of the leading non-analytic correction exponent $\Delta_1 = 1.160 \pm 0.025$, which indicates that the non-analytic correction terms alone are not sufficient to explain the deviation. Each of the parts (*b*), (*c*) and (*d*) of figure 7, shows the same area in the Δ_1–γ-space for a different trial value of p_c (indicated in the figure). We include the near central Padé approximants of highest order in the analysis, as detailed in the legend. In M1 one plots estimates of Δ_1 as a function of input values of γ, which leads to one line of data points for each Padé approximant. In figure 7(*c*) of these

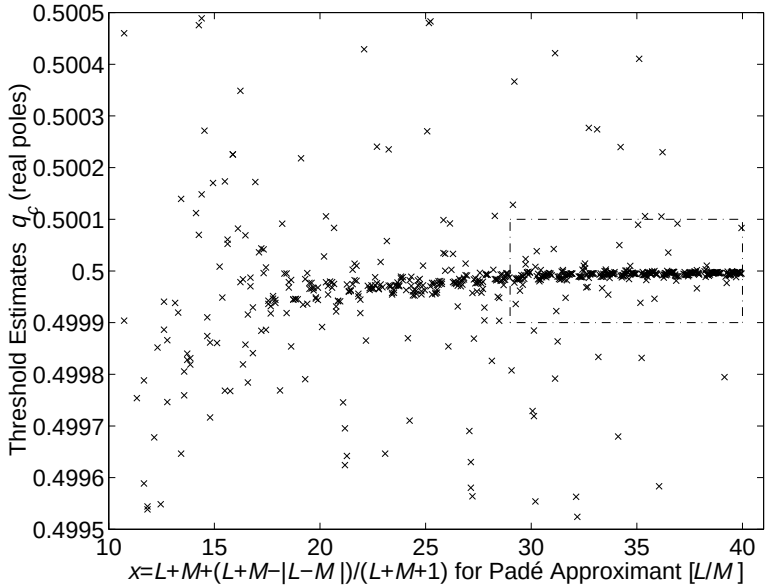

(*a*)

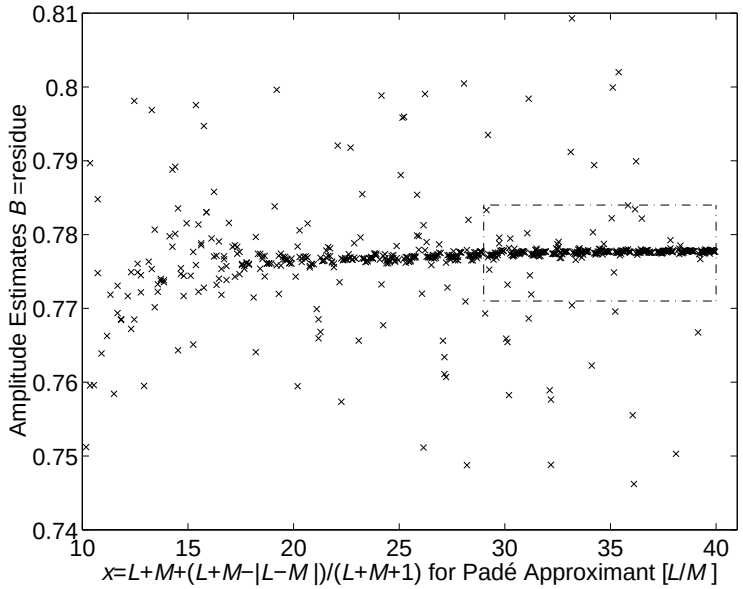

(*b*)

Figure 5. Estimates for q_c (*a*) and B (*b*) from the B-amplitude series in the bond-percolation (bond-counting) model. No Euler transformation was applied. Each point in the plot corresponds to a particular Padé approximant $[L/M]$, where L and M relate to the number on the x-axis as given in the label. Final estimates were calculated from these kind of plots as explained in the body of the text. The points that were included in the average are those within the boxed areas. The resulting numbers are summarized in table 4.

Table 4. Summary of the numerical values for the bond-percolation (bond-counting) model. Whenever this paper includes a plot for a line of data, the corresponding figure is given as reference. Otherwise we show four numbers, which are, in the given order, the lowest and highest order of Padé approximants as well as lower and upper bound for estimates included in the average. n is the number of individual estimates that were averaged.

Reference	n	q_c	Δq_c	β	$\Delta\beta$
Figure 3[a]	213	0.499 35	0.000 72	0.134 4	0.003 2
Reference	n	q_c	Δq_c	β	$\Delta\beta$
Figure 4[a]	453	0.499 978	0.000 087	0.777 1	0.002 1
Figure 5[b]	295	0.499 993 5	0.000 019 1	0.777 71	0.000 95
Figure 6[c]	360			0.778 00	0.000 60
Reference	n	p_c	Δp_c	Γ_2	$\Delta\Gamma_2$
Figure 8[a]	68	0.499 55	0.000 61	0.073 2	0.001 9
Figure 9(a)[b]	43	0.499 86	0.000 65	0.074 5	0.003 4
12 18 0.073 0.076[c]	68			0.074 84	0.000 41
Reference	n	p_c	Δp_c	ξ_0	$\Delta\xi_0$
Figure 9(b)[b]	60	0.499 33	0.000 70	0.522 3	0.005 4
8 14 0.5 0.56[c]	48			0.526 7	0.006 4
Reference	n			$B^2\xi_0^2/\Gamma_2$	$\Delta(B^2\xi_0^2/\Gamma_2)$
Figure 10[c]	31			2.215	0.040

[a] From pole–residue plot.
[b] From plot of estimate from residue versus order of Padé approximant.
[c] From biased evaluation of Padé approximants.

Table 5. Summary of the numerical values for the bond-percolation (site counting) model. See also caption of table 4.

Reference	n	p_c	Δp_c	γ	$\Delta\gamma$
Figure 11[a]	48	0.499 7	0.001 4	2.385	0.040
Reference	n	p_c	Δp_c	Γ_2	$\Delta\Gamma_2$
Figure 12(a)[b]	50	0.499 82	0.000 43	0.119 46	0.002 36
11 16 0.118 0.121[c]	50			0.119 63	0.000 35
Reference	n	p_c	Δp_c	ξ_0	$\Delta\xi_0$
Figure 12(b)[b]	46	0.499 93	0.000 18	0.369 96	0.000 96
10 15 0.368 0.374[c]	39			0.370 32	0.000 60

[a] From pole–residue plot.
[b] From plot of estimate from residue versus order of Padé approximant.
[c] From biased evaluation of Padé approximants.

lines are distributed symmetrically around the point they all cross. How well they converge can only be seen if one enlarges the convergence area (inset in (c)). In (b) and (d), with lower and higher trial values of p_c, the convergence degrades and most lines shift to the right or left side of the point of convergence (see [21] regarding graphical methods of series analysis). Thus the estimates are read from figure 7(c) with error estimates set by (b) and (d).

It is known that *analytic* corrections are observed as shifts in the critical threshold. This is probably also the case here. In such cases M1 gives an effective mixture of both corrections [22].

Table 6. Summary of the numerical values for the site-percolation model. See also caption of table 4.

Reference	n	q_c	Δq_c	B	ΔB
Figure 13(a)[a]	97	0.407 246 4	0.000 007 2	0.910 09	0.000 44
24 31 0.91 0.911[b]	174			0.910 556	0.000 12
Reference	n	p_c	Δp_c	Γ_2	$\Delta\Gamma_2$
Figure 13(b)[a]	43	0.592 70	0.000 29	0.097 22	0.001 50
18 25 0.094 0.102[b]	108			0.097 92	0.000 51
Reference	n	p_c	Δp_c	ξ_0	$\Delta\xi_0$
14 17 0.51 0.53[a]	34	0.593 27	0.000 32	0.5202	0.0028
14 17 0.5 0.53[b]	27			0.5144	0.0041
Reference	n			$B^2\xi_0^2/\Gamma_2$	$\Delta(B^2\xi_0^2/\Gamma_2)$
14 16 2 2.5[b]	20			2.231	0.086

[a] From plot of estimate from residue versus order of Padé approximant.
[b] From biased evaluation of Padé approximants.

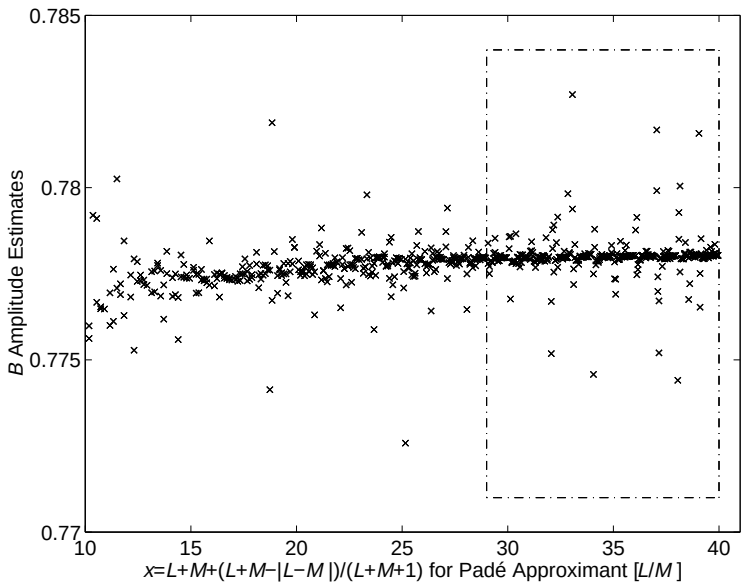

Figure 6. Estimates for B for the bond-percolation (bond-counting) model from biased evaluation of Padé approximants to $P(q)(q_c - q)^{-\beta}$. The numbers resulting from averaging over the boxed area are summarized in table 4. See the caption of figure 5 for further explanation.

One cause for analytic corrections is the Euler transformation and we found that the deviation indeed depends on the value of p_n. Without Euler transformation, however, pole–residue points decrease in number and spread over the range of the reported deviation. The systematic deviation is covered by our error estimates.

To analyse for the critical amplitude Γ_2 we transform the original series to one approximating $(M_2/p)^{1/\gamma}$, using our knowledge of the exact γ. Figure 8 shows the excellent convergence obtained in the pole–residue plot, and figure 9(a) shows Γ_2 estimates, plotted

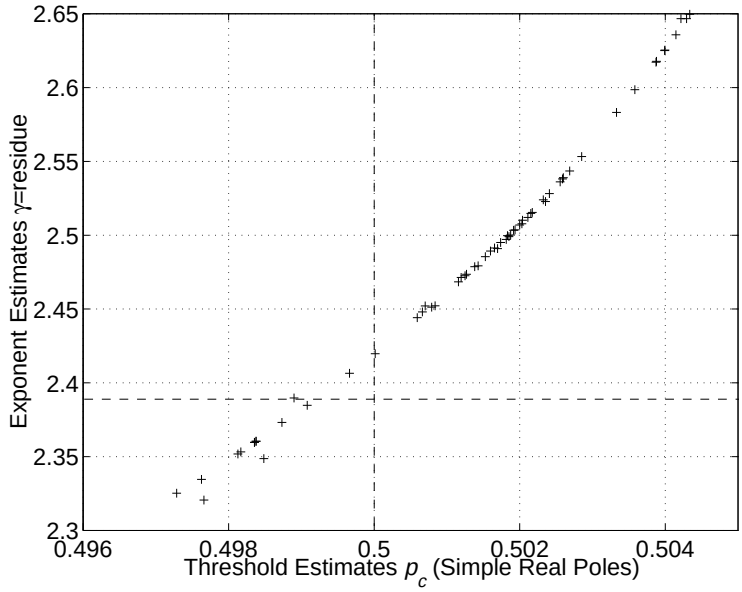

(*a*)

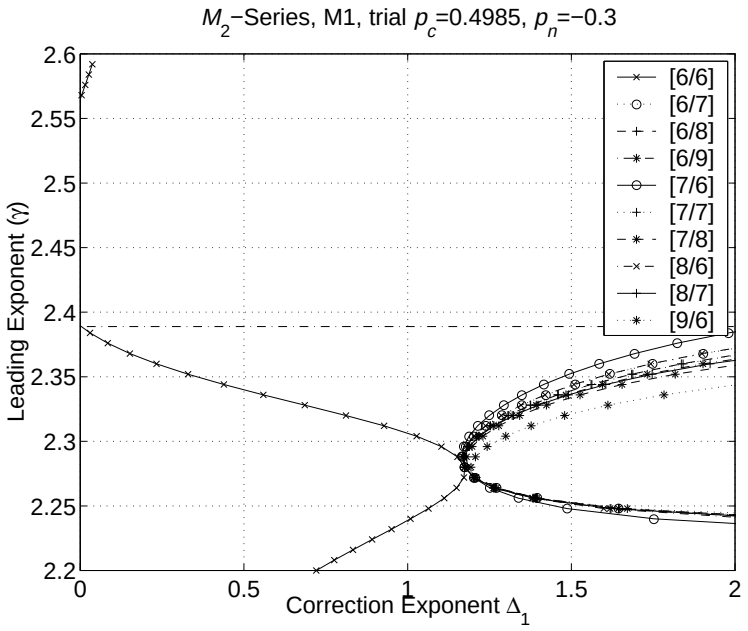

(*b*)

Figure 7. (*a*) Pole–residue plot from a Dlog Padé analysis of the series for $M_2(p)/p$ in the bond-percolation (bond-counting) model. The dashed lines indicate the known values. One sees that the line of data points does not pass exactly through the correct point when using an Euler transformation with $p_n = -0.3$. (*b*)–(*d*) Examination of non-analytic corrections for $M_2(p)$ in the same model using the M1 technique. We show the plots for three different trial values of p_c as indicated. Best convergence is achieved for $p_c = 0.4990$ in (*c*). Hence this analysis could not resolve the small deviation from the known critical parameters.

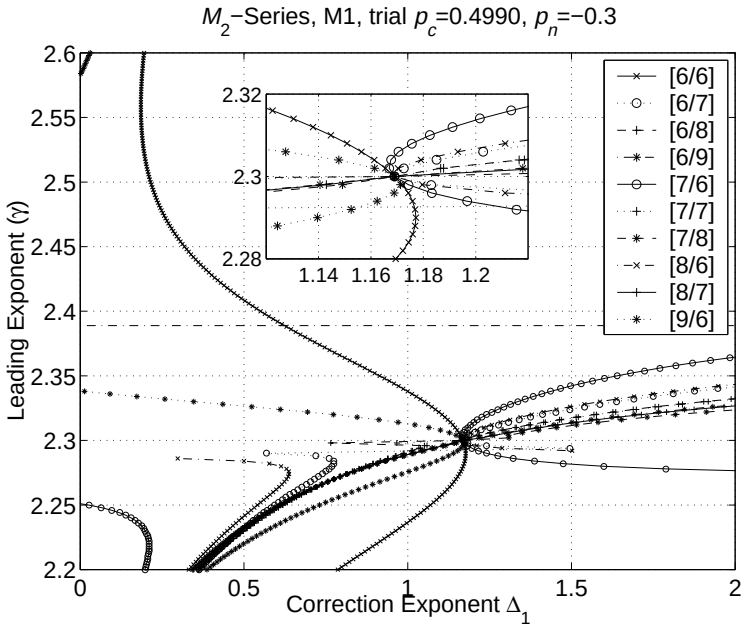

(*c*)

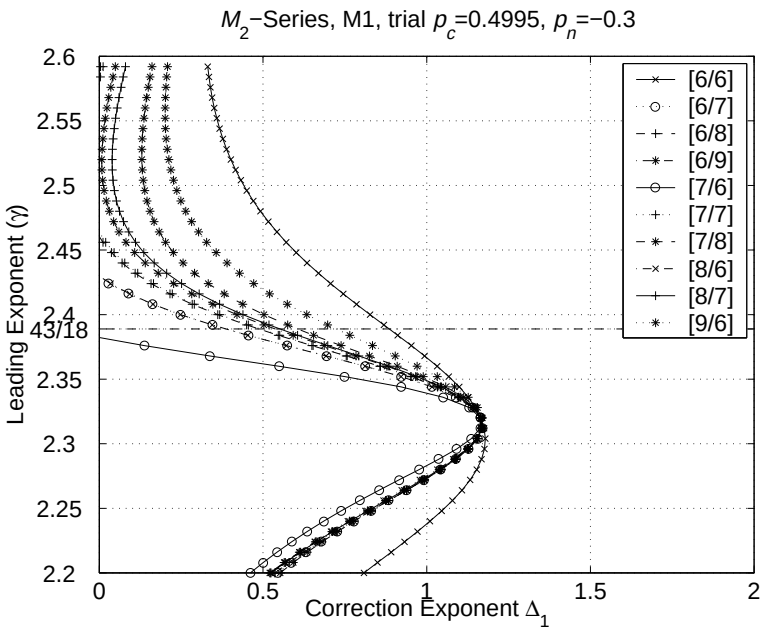

(*d*)

Figure 7. (Continued)

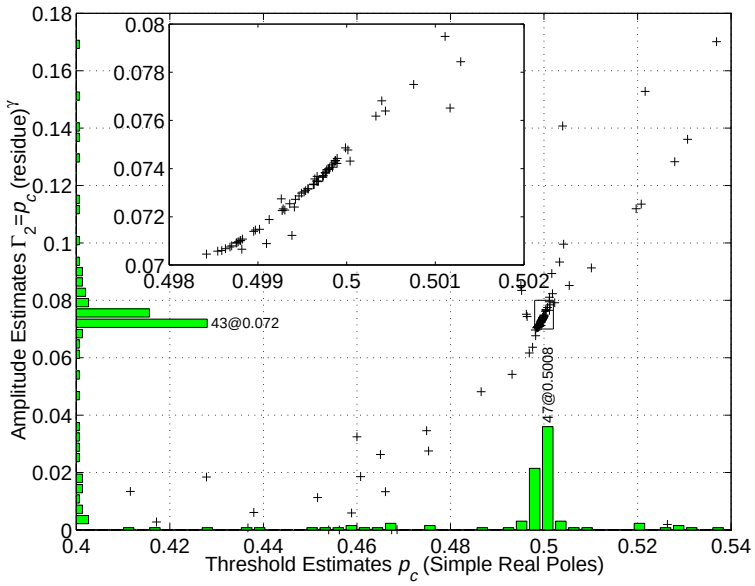

Figure 8. Pole–residue plot from a Padé analysis of the Γ_2-amplitude series in the bond-percolation (bond-counting) model. No Euler transformation was applied. See the caption of figure 3 for further explanation.

against the order of the Padé approximants. The results from averaging over the boxed area are included in table 4. There we also give the results from the biased Padé analysis of the series to $(M_2/p)^{1/\gamma}(p_c - p)$.

Series for $\xi^2(p)$. The original 14-term $\xi^2(p)$-series behaves excellently for its limited length, judged from the Dlog Padé analysis, in the sense that the line of data points is well converged and passes exactly through the known point $(p_c, 2\nu)$ within the bounds set by scattering. We followed the usual sequence of analysis as described above.

To obtain the amplitude ξ_0 we use the transformed series for $(\xi^2/p)^{1/(2\nu)}$. Estimates for the amplitude ξ_0 are hence calculated from the residues of simple real poles, as $\xi_0 = (\text{residue}^{2\nu} p_c)^{1/2}$. The series needs to be Euler transformed with p_n around -0.3 to behave well. Plots of the relevant estimates against the order of Padé approximants are shown in figure 9(*b*). The results from this figure and from biased analysis for $\xi^2(p_c - p)^{2\nu}$ are again summarized in table 4.

In the context of biased estimates, a way to directly analyse the series for the amplitude ratio $B^2\xi_0^2/\Gamma_2$ is useful. By combining the original series we get an expansion for the quantity $[P^2\xi^2/M_2](x)$; here x denotes the expansion variable which was p or q for the original series. Scaling theory predicts that not only the leading singular terms cancel out, leaving the amplitude combination as constant 'background', but also the analytic corrections cancel [23] and the leading non-analytic correction term is smaller than in the original series [4]. We show a plot of such analysis in figure 10. The obtained average $B^2\xi_0^2/\Gamma_2 = 2.215 \pm 0.040$ is more precise than the value from individual amplitudes (table 7), and according to the above scaling prediction less prone to systematic errors than biased estimates for the individual amplitudes.

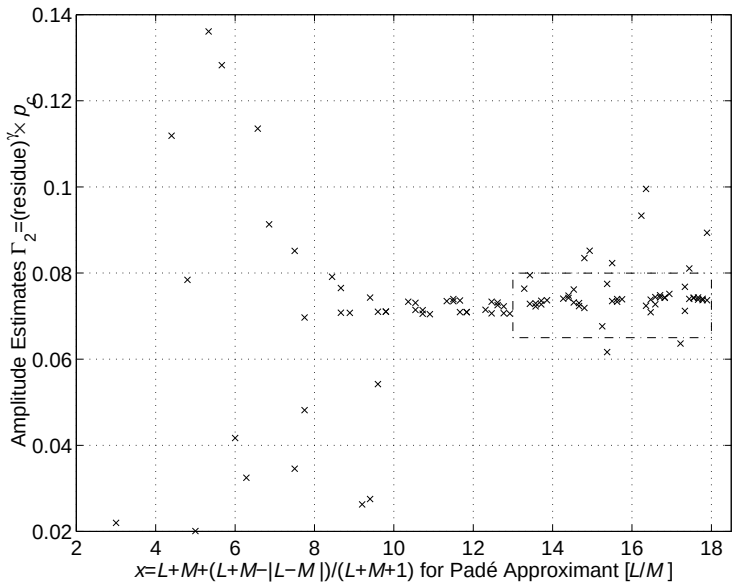

(*a*)

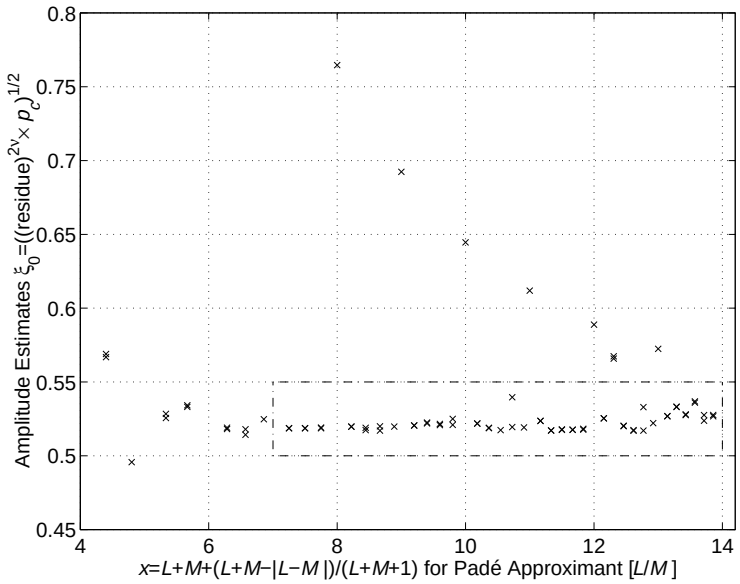

(*b*)

Figure 9. (*a*) Estimates for Γ_2 from the Γ_2-amplitude series in the bond-percolation (bond-counting) model. No Euler transformation was applied. (*b*) Estimates for ξ_0 from the ξ_0-amplitude series in the bond-percolation (bond-counting) model. We used an Euler transformation with $p_n = -0.3$. See the caption of figure 5 for further explanation.

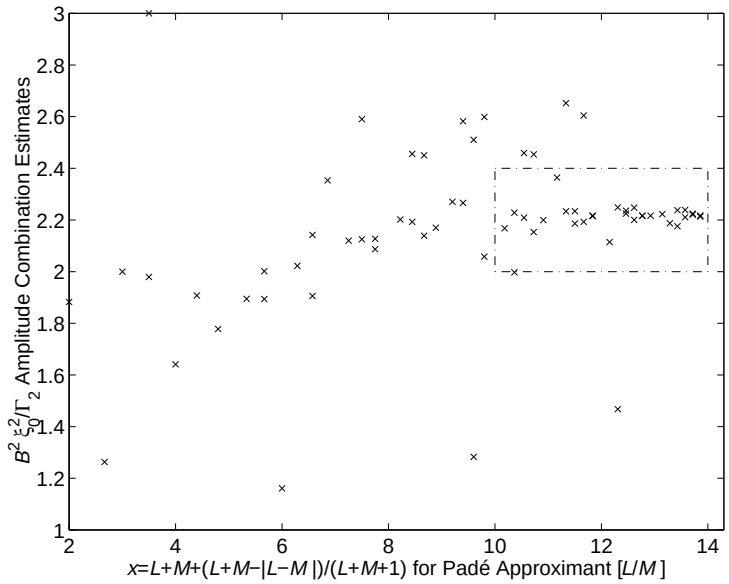

Figure 10. Direct estimates for the amplitude combination $B^2\xi_0^2/\Gamma_2$ for the bond-percolation (bond-counting) model from biased evaluation of Padé approximants to $[P^2\xi^2/M_2](x)$. The numbers resulting from averaging over the boxed area are summarized in table 4. See the caption of figure 5 for further explanation.

4.2. Bond percolation with site counting

In the case of bond percolation with site counting the high concentration series of $P(q)$ available to us is too short to be useful. Hence we analyse only the series for $M_2(p)$ and $\xi^2(p)$, presented in table 2, and use the value of B from Monte Carlo simulations (see below in section 5) to calculate the universal combination. For the analysis of the series we follow the same schedule as in the bond-counting case, so we do not repeat the details here.

Both the series for $M_2(p)$ and for $\xi^2(p)/p$ cause no problems in the Dlog Padé analysis if Euler transformations are applied. Convergence of data points is good and their lines pass precisely through the correct point of known exponent and threshold within the limit of scattering. Figure 11 shows a plot for $M_2(p)$ as a typical example.

As amplitude series we use series transformed in the same (or very similar) way described in section 4.2, followed by Padé analysis. The final results are obtained from plots of the amplitude estimates (calculated from residues) as a function of the total order of the Padé approximants, such as figures 12(*a*) and (*b*). We also give biased estimates for Γ_2 and ξ_0 in table 5, together with all numerical results from this section.

4.3. Site percolation

Again we follow a very similar schedule of analysis for the three series for $P(q)$, $M_2(p)$ and $\xi^2(p)$ listed in table 3.

All the original series behave well, in the common sense, in Dlog Padé analysis, occasionaly combined with Euler transformations. The same is true for the amplitude series. We get good convergence in the pole–residue plots, and the highest concentration of data points is indeed located around the known p_c.

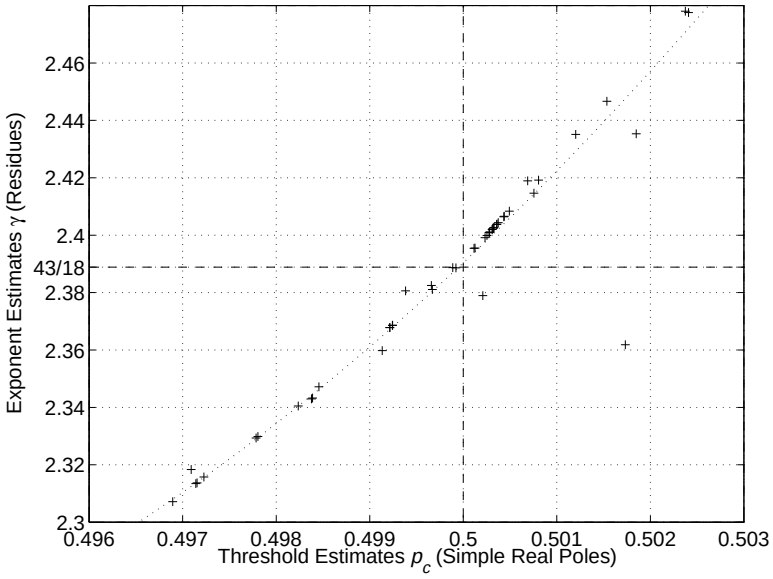

Figure 11. Pole–residue plot from a Dlog Padé analysis of the series of $M_2(p)$ in the bond-percolation (site-counting) model. We used an Euler transformation with $p_n = -0.3$. The numbers resulting from averaging over the displayed area are summarized in table 5.

The final values for the amplitudes are again obtained from plots of estimates as a function of the total order of the Padé approximants (figure 13 for B and Γ_2), both from biased and unbiased analysis.

Direct biased estimation of the amplitude combination leads to $B^2\xi_0^2/\Gamma_2 = 2.231 \pm 0.086$. Note that here (for site percolation on the square lattice) $p_c \neq q_c$. Hence we first transform the individual series to a new variable x, such that $x_c = 1$. This produces a factor of $(q_c/p_c)^{5/18}$ in the estimates from the combined series.

5. Monte Carlo simulations

For the Monte Carlo simulations, we used a standard Hoshen–Kopelman algorithm [1] on square bond lattices of size 6000×6000 to $20\,000 \times 20\,000$ with free boundary conditions. Random integers of 64 bits were produced by multiplication with 16 807 and omission of leading bits after overflow. Up to 2560 samples were simulated simultaneously on a Cray-T3E, with each of the 256 processors looking at ten different lattices and requiring about 0.4 μs per site. For the evaluation of M_2 also the largest cluster was taken into account since we needed this moment only below p_c. All clusters were characterized by the number of sites in them, not by the number of bonds.

The evaluation of the order parameter amplitude B was difficult because of non-monotonic size effects, also known from other phase transitions. For the 6000×6000 lattices, the product $P(p-p_c)^{-\beta}$, which should approach B from equation (4), decreases with increasing $p-p_c$ for $10^{-6} < p - p_c < 10^{-4}$, reaches a minimum at 0.0002, then increases to a maximum at about 0.01, and then slowly decreases. Figure 14 compares this effect with that at size 7000×7000 and $20\,000 \times 20\,000$; the larger the lattice is the closer we have to get to the critical point to see the deviations. We thus concluded $B \simeq 1.39$ from figure 14 by extrapolation of the linear p-dependence somewhat above p_c, and not $B \simeq 1.30$ from the data closest to p_c.

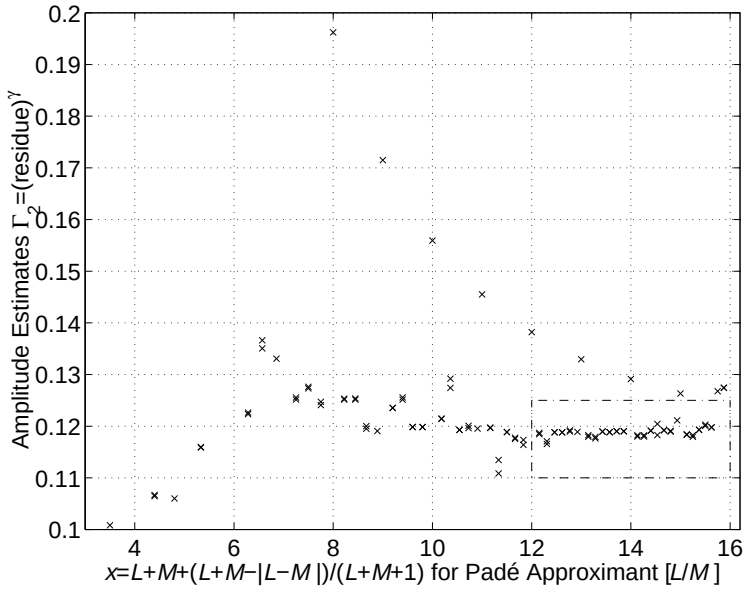

(*a*)

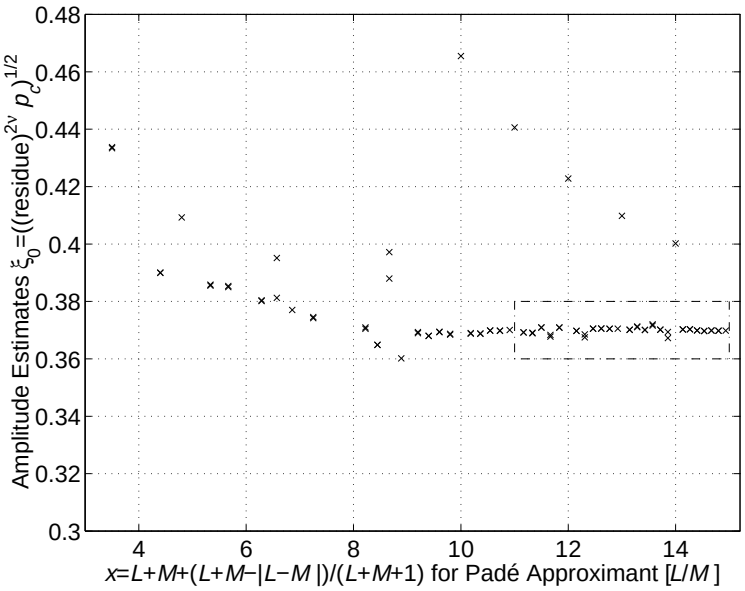

(*b*)

Figure 12. (*a*) Estimates for Γ_2 from the Γ_2-amplitude series in the bond-percolation (site-counting) model. We used an Euler transformation with $p_n = -0.3$. (*b*) Estimates for ξ_0 from the ξ_0-amplitude series in the same model. See the caption of figure 5 for further explanation. The numbers resulting from averaging over the boxed area are summarized in table 5.

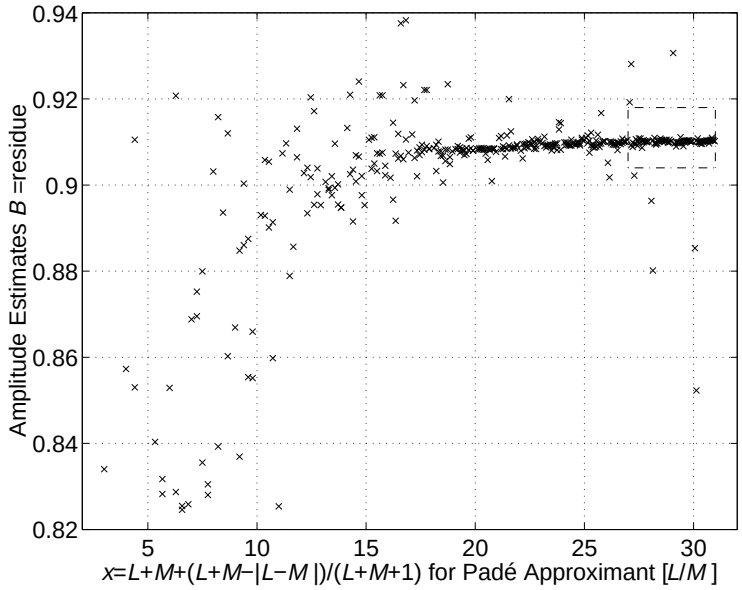

(*a*)

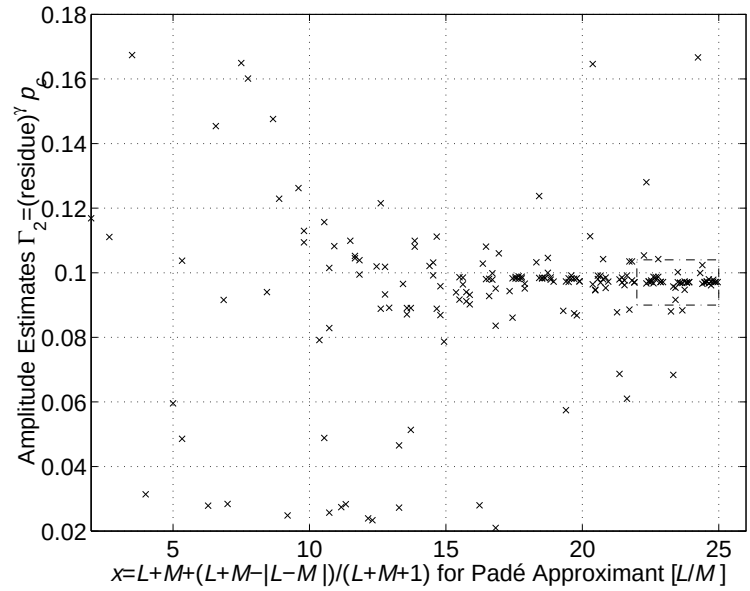

(*b*)

Figure 13. (*a*) Estimates for B from the B-amplitude series in the site-percolation model. No Euler transformation was applied. (*b*) Estimates for Γ_2 from the Γ_2-amplitude series. No Euler transformation was applied. See the caption of figure 5 for further explanation. The numbers resulting from averaging over the boxed area are summarized in table 6.

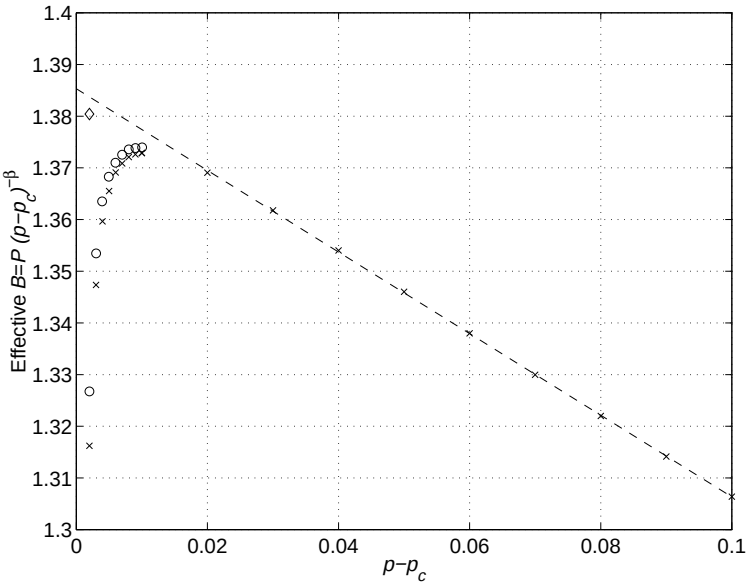

Figure 14. Scaled order parameter $P(p - p_c)^{-\beta}$ for bond percolation with site counting on 6000×6000 ($\times$) and 7000×7000 ($\bigcirc$) square lattices as well as $20\,000 \times 20\,000$ ($\diamond$). It approaches $B \simeq 1.39$ for 'infinite' lattices and $p \to p_c$. (- - - -) is a linear fit to '$\times$' with $p - p_c > 0.01$.

Table 7. The results for critical amplitudes and the universal combination thereof. Comparison of the different models.

Model	Ref.	$B = \Gamma_1$	Γ_2	ξ_0	$B^2\xi_0^2/\Gamma_2$
Square lattice					
Site percolation	a	0.910 ± 0.009	0.102 ± 0.001	0.520 ± 0.005	2.195 ± 0.064
	b	$0.910\,09 \pm 0.000\,44$	$0.097\,22 \pm 0.001\,50$	$0.520\,2 \pm 0.0028$	2.305 ± 0.043
	c	$0.910\,56 \pm 0.000\,12$	$0.097\,92 \pm 0.000\,51$	$0.514\,4 \pm 0.0041$	2.240 ± 0.038
	d				2.231 ± 0.086
Bond percolation	e	1.39 ± 0.01	0.12 ± 0.01		2.20 ± 0.19[g]
(site counting)	f	$1.388\,2 \pm 0.000\,4$	$0.119\,48 \pm 0.000\,10$	$0.371\,1 \pm 0.0002$	2.221 ± 0.003
	b		$0.119\,46 \pm 0.002\,36$	$0.369\,96 \pm 0.000\,96$	2.208 ± 0.045[g]
	c		$0.119\,63 \pm 0.000\,35$	$0.370\,32 \pm 0.000\,60$	2.209 ± 0.010[g]
Bond percolation	b	$0.777\,71 \pm 0.000\,95$	$0.074\,5 \pm 0.003\,4$	$0.522\,3 \pm 0.0054$	2.215 ± 0.111
(bond counting)	c	$0.778\,00 \pm 0.000\,60$	$0.074\,84 \pm 0.000\,41$	$0.526\,7 \pm 0.0064$	2.244 ± 0.056
	d				2.215 ± 0.040
Triangular lattice					
Site percolation	a	0.780 ± 0.008	$0.072\,0 \pm 0.0007$	0.520 ± 0.005	2.285 ± 0.068

[a] From Monte Carlo simulation in [24].
[b] From plot of estimate versus order of Padé approximant, this work.
[c] From biased evaluation of Padé approximants, this work.
[d] From direct evaluation of Padé approximants to combined series, this work.
[e] From Monte Carlo simulation, this work.
[f] From Monte Carlo simulation by [28].
[g] Combining numbers from series and Monte Carlo.

6. Summary of results and discussion

In table 7 we present the values obtained for the various amplitudes and their combinations. It contains results from the analysis of the new series presented in this paper as well as analysis

of series obtained from [8]. From each series we obtained two estimates, unbiased and biased, as detailed in section 4. They agree in all cases and usually the biased evaluation of Padé approximants results in smaller error margins. However, systematic errors, which can be due to corrections to the leading singular behaviour, may be larger than these margins, which were calculated as standard deviations from averaging over a subset of all the different approximants. The unbiased estimates of the amplitudes also yield estimates for the thresholds, which agree with the accurately or exactly known values (tables 4–6). The error margin would have to be increased slightly to include the known value only in two cases. Thus is seems reasonable to set our confidence limits to the unbiased averages with two standard deviations as error margins.

For bond percolation with bond counting and for site percolation, series for all three quantities $P(q), M_2(p)$ and $\xi(p)$ are available, allowing us to calculate the amplitude combination directly from approximants to the combined series. In principle this should be the most accurate and reliable way of analysis. In practice, the results of such calculations agree with the former but do not have higher accuracy. This is not surprising, since the combined series is limited to the length of the shortest individual one, and our series differed in length considerably.

Conway and Guttmann [8] also obtained amplitude estimates from their series using biased evaluation. With the same technique we reproduce their values (and error estimates, see table 7), apart from minor deviations, which are likely due to different ranges of Padé approximants included in the average. For the comparison we converted their numbers to our definitions as $B_{\text{this paper}} = Bp_c^{1-\beta}$ and $\Gamma_2 = C^+ p_c^{\gamma+1}$.

The table further contains estimates from Monte Carlo studies. Those for site percolation were reported in [24] (for ξ_0 see also [25]), those for bond percolation in the previous section. Where both Monte Carlo and estimates from series analysis are available, they agree within the stated errors (with one marginal exception). Note that the presumably most accurate value for the amplitude combination is close to $\frac{20}{9} \approx 2.222$, a value which agrees with all the listed estimates (except for one from biased evaluation, see the discussion above).

Overall, we have confirmed numerically that the amplitude combination $B^2\xi_0^2/\Gamma_2$ is indeed a universal quantity for two-dimensional percolation; all the measured values are consistent with the value of 2.23 ± 0.10. We have also emphasized the importance of choosing the correct unit of length in order to test this result.

The literature contains additional results for B and Γ_2 from series analysis [26, 27]. However, the values given by Sykes *et al* for site and bond percolation (bond counting) on the square lattice do not agree with those from [8] and ours. Taking their values anyway, one can combine them with our value of $B^2\xi_0^2/\Gamma_2$ to deduce the values $\xi_0 = 0.487 \pm 0.022$, 0.461 ± 0.021, 0.440 ± 0.022, and 0.461 ± 0.021 for site percolation on the triangular lattice, bond percolation on the triangular lattice, site percolation on the honeycomb lattice, and bond percolation on the honeycomb lattice, respectively. Note that Γ_2 and ξ_0 for site percolation on the triangular lattice also do not agree with those from the Monte Carlo simulations in [24]. Thus, Sykes *et al*'s values may have a larger error than cited, probably due to the shorter series used there.

Acknowledgments

We acknowledge discussions with Joan Adler, Iksoo Chang, A Brooks Harris, Zvi Lev and Michael E Fisher. We thank P Grassberger for advance information on his Monte Carlo results and the German Israeli Foundation for support. DS thanks the Jülich Supercomputer Center for time on their Cray-T3E.

References

[1] Stauffer D and Aharony A 1994 *Introduction to Percolation Theory* (London: Taylor and Francis)
[2] Sahimi M 1994 *Application of Percolation Theory* (London: Taylor and Francis)
[3] Bunde A and Havlin S 1996 *Fractals and Disordered Systems* (Berlin: Springer)
[4] Privman V, Hohenberg P C and Aharony A 1991 *Phase Transitions and Critical Phenomena* vol 14, ed C Domb, M S Green and J L Lebowitz (New York: Academic) p 1
[5] Martin J L 1974 *Phase Transitions and Critical Phenomena* vol 2, ed C Domb and M S Green (New York: Academic) p 97
[6] Redelmeier D H 1981 *Discrete Math.* **36** 191
[7] Redner S 1982 *J. Stat. Phys.* **29** 309
[8] Conway A R and Guttmann A J 1995 *J. Phys. A: Math. Gen.* **28** 891
[9] Privman V, Family F and Margolina A 1984 *J. Phys. A: Math. Gen.* **17** 2837
[10] Daboul D *PhD Thesis* Tel Aviv University
[11] Wan C C, Harris A B and Adler J 1991 *J. Appl. Phys.* **69** 5191
[12] Adler J *et al* 1990 *Phys. Rev.* B **41** 9183
[13] Ziff R M, Finch S R and Adamchik V 1997 *Phys. Rev. Lett.* **79** 3447
[14] Ziff R M 1992 *Phys. Rev. Lett.* **69** 2670
[15] Guttmann A J 1989 *Phase Transitions and Critical Phenomena* vol 13, ed C Domb and J L Lebowitz (New York: Academic) pp 1–234
[16] Adler J, Moshe M and Privman V 1982 *Phys. Rev.* B **26** 1411
[17] Privman V 1983 *J. Phys. A: Math. Gen.* **16** 3097
[18] Adler J 1996 *Annual Reviews of Computational Physics* vol 4, ed D Stauffer (Singapore: World Scientific) p 241
[19] Pearce C J 1978 *Adv. Phys.* **27** 89
[20] Jensen I 1999 *J. Phys. A: Math. Gen.* **32** 5233
[21] Adler J, Chang I and Shapira S 1993 *Int. J. Mod. Phys.* C **4** 1007
[22] Adler J and Enting I G 1984 *J. Phys. A: Math. Gen.* **17** 2233
[23] Aharony A and Fisher M E 1983 *Phys. Rev.* B **27** 4394
[24] Aharony A and Stauffer D 1997 *J. Phys. A: Math. Gen.* **30** L301
[25] Hoshen J 1997 *J. Phys. A: Math. Gen.* **30** 8459
[26] Sykes M F, Gaunt D S and Glen M 1976 *J. Phys. A: Math. Gen.* **9** 97
[27] Sykes M F, Gaunt D S and Glen M 1976 *J. Phys. A: Math. Gen.* **9** 725
[28] Grassberger P 1999 Private communication